Atmos. Chem. Phys. Discuss., 11, 4167–4198, 2011
www.atmos-chem-phys-discuss.net/11/4167/2011/
doi:10.5194/acpd-11-4167-2011

Atmospheric Chemistry and Physics Discussions

Zonal asymmetries in middle atmospheric ozone and water vapour derived from Odin satellite data 2001–2010

A. Gabriel[1], **H. Körnich**[2], **S. Lossow**[3], **D. H. W. Peters**[1], **J. Urban**[3], and **D. Murtagh**[3]

[1]Leibniz-Institute for Atmospheric Physics of the University Rostock e.V., Schlossstr. 6, 18225 Kühlungsborn, Germany
[2]Department of Meteorology, Stockholms University, 106 91 Stockholm, Sweden
[3]Chalmers University of Technology, Department of Earth and Space Sciences, Hörsalsvägen 11, 41296 Göteborg, Sweden

Received: 2 December 2010 – Accepted: 21 January 2011 – Published: 4 February 2011

Correspondence to: A. Gabriel (gabriel@iap-kborn.de)

Published by Copernicus Publications on behalf of the European Geosciences Union.

Abstract

Based on Odin satellite data 2001–2010 we investigate stationary wave patterns in middle atmospheric ozone (O_3) and water vapour (H_2O) as indicated by their seasonal long-term means of the zonally asymmetric components $O_3^* = O_3$-$[O_3]$ and $H_2O^* = H_2O$-$[H_2O]$ ($[O_3]$, $[H_2O]$: zonal means). At mid- and polar latitudes of Northern and Southern Hemisphere, we find a pronounced wave one pattern in both constituents. In the Northern Hemisphere, the wave one patterns increase during autumn, maintain their strength during winter and decay during spring, with maximum amplitudes of about 10–20% of zonal mean values. During winter, the wave one in stratospheric O_3^* is characterized by a maximum over North Pacific/Aleutians and a minimum over North Atlantic/Northern Europe and by a double-peak structure with enhanced amplitude in the lower and in the upper stratosphere. The wave one in H_2O^* extends from lower stratosphere to upper mesosphere with a westward shift in phase with increasing height including a jump in phase at upper stratosphere altitudes. In the Southern Hemisphere, similar wave one patterns occur during southern spring when the polar vortex breaks down. Based on a simplified tracer transport approach we explain these wave patterns as a first-order result of zonal asymmetries in mean meridional transport by geostrophically balanced winds, which were derived from combined temperature profiles of Odin, and ECMWF (European Centre of Medium-Range Weather Forecasts) Reanalysis data (ERA Interim). Further influences which may contribute to the stationary wave patterns, e.g. eddy mixing processes or temperature-dependent chemistry, are discussed.

ACPD

11, 4167–4198, 2011

1 Introduction

Quasi-stationary planetary wave patterns in temperature or geopotential are a well known feature of the extra-tropical middle atmosphere (e.g., Andrews et al., 1987). Planetary waves play an essential role in driving the zonal mean transport by Brewer-Dobson circulation and eddy mixing processes, i.e. the zonal mean meridional transport of trace gases from tropics to mid- and polar latitudes (Tung, 1982; Holton, 1985; Andrews et al., 1987). Important efforts have been made to understand and to quantify the contributions of the transport processes to the mean seasonal cycle and to the long-term variations in the zonal mean distributions of stratospheric ozone and water vapour (WMO, 2007; SPARC Report No. 2, 2000). However, the three-dimensional structure of stationary wave patterns in stratospheric ozone and stratospheric and mesospheric water vapour has been investigated only very sparsely up to now. The aim of the presented paper is to derive the three-dimensional stationary wave patterns in ozone and water vapour from Odin satellite data 2001–2010, covering altitude ranges of ~10–75 km for ozone and ~15–110 km for water vapour.

In the Northern Hemisphere, usually a quasi-stationary wave pattern with a pronounced zonal wave number one (wave one pattern) occurs during winter which is related to zonal asymmetries in the stratospheric polar vortex, i.e. to Aleutian high and polar low anomalies in geopotential height (note that the centre of the polar vortex occurs most frequently over North-Eastern Europe/Western Siberia, as found by Waugh and Randel, 1999, and Karpetchko et al., 2005). Other wave modes (particularly wave two and wave three) develop mainly as a precursor of and during stratospheric warming events or during final vortex break-up periods. The common understanding is that planetary waves, which are forced in the troposphere by large mountain ridges, land-ocean contrast or longitude-dependent heat sources, propagate vertically within mean westerly but not easterly flow into the middle atmosphere where they generate the quasi-stationary wave patterns (Charney and Drazin, 1961). In the mesosphere, zonal asymmetries in gravity wave breaking may also play an important role in configuring stationary wave patterns (e.g., Smith, 2003).

ACPD
11, 4167–4198, 2011

Mean concentrations of water vapour (H_2O) decrease very rapidly in the upper troposphere/lowermost stratosphere region (Holton and Gettelmann, 2001) and increase then again up to maximum values around stratopause because of oxidation of methane (CH_4), which is transported from troposphere into stratosphere (e.g., Brasseur and Solomon, 1995; SPARC Report No. 2, 2000). Based on satellite data from the Halogen Occultation Experiment (HALOE) on the Upper Atmosphere Research Experiment (UARS), Randel et al. (1998) reveal the influence of zonal mean transport processes on the seasonal cycle and long-term variations of stratospheric CH_4 and H_2O. In the mesosphere, where H_2O is also a nearly inert tracer, the zonal mean H_2O distribution results mainly from the mean annual cycle in zonal mean meridional transport, as shown by Lossow et al. (2009) diagnosing Odin satellite data and chemistry-climate model calculations. The observed increase of zonal mean stratospheric water vapour during the last decades may have a substantial influence on atmospheric circulation patterns via radiation perturbations (Joshi et al., 2006). However, three-dimensional planetary wave patterns or zonal asymmetries in water vapour have not been considered up to now.

Two- and three-dimensional model investigations have shown that planetary waves have a strong influence on ozone transport and temperature-dependent ozone chemistry (e.g., Austin and Butchart, 1992; Solomon et al., 1998; Kinnersley and Tung, 1998; Gabriel and Schmitz, 2003). The influence of planetary wave patterns on the longitude-dependent distribution of total column ozone was demonstrated based on simplified approaches of tracer transport for the lower stratosphere (Hood and Zaff, 1995; Peters and Entzian, 1996, 1999). Stationary wave one patterns or zonal asymmetries in stratospheric ozone were found in assimilated ozone of European Centre of Medium-Range Weather Forecasts (ECMWF) Reanalysis data (Gabriel et al., 2007), and their decadal variations were found to be coherent with decadal variations in upper tropospheric geopotential height (Peters et al., 2008). Recently numerical model calculations have shown that the zonal asymmetries in stratospheric ozone can significantly modify planetary wave propagation and atmospheric circulation (Sassi et al.,

ACPD
11, 4167–4198, 2011

2005; Gabriel et al., 2007; Crook et al., 2008; Gillet et al., 2009; Waugh et al., 2009). However, the processes responsible for the quasi-stationary wave patterns in observed stratospheric ozone and its long-term changes are not well understood up to now.

During the last two decades more and more accurate satellite data are available which provide a new perspective to investigate the three-dimensional wave patterns. The Odin satellite, which was launched in 2001 and which is currently still in orbit, provide such suitable information throughout the middle atmosphere (Urban et al., 2007, Lossow et al., 2008, 2009; Jones et al., 2009). We use this data to derive long-term means of quasi-stationary wave patterns in stratospheric ozone and stratospheric and mesospheric water vapour, as indicated by the zonal asymmetries $O_3^* = O_3\text{-}[O_3]$ and $H_2O^* = H_2O\text{-}[H_2O]$ ($[O_3]$, $[H_2O]$: zonal means). The results are presented in Sect. 2. In Sect. 3 we estimate the contribution of zonally asymmetric meridional transport in configuring these stationary wave patterns based on a simplified transport approach for an inert tracer. Section 4 concludes with summary and discussion.

2 Diagnosis of zonal asymmetries in ozone, water vapour and temperature

2.1 Data

The Odin satellite was launched in 2001 as a joint venture of Sweden, Canada, Finland and France (Murtagh et al., 2002), and it is currently still in orbit as an European Space Agency (ESA) third party mission. Odin is polar orbiting (82.5° S to 82.5° N) and sun synchronous, and it includes the Sub-Millimetre Radiometer (SMR) and the Optical Spectrograph InfraRed Imager System (OSIRIS) providing, amongst others, measurements of ozone (altitude range: ~20–75 km), water vapour (~15–110 km) and temperature (~50–90 km). Some more details of Odin and the retrievals can be found, for example, in Urban et al. (2005) and Lossow et al. (2007). The Odin data have been used widely to diagnose middle atmospheric ozone and water vapour (e.g., Urban et al., 2007; Lossow et al., 2008, 2009; Jones et al., 2009).

ACPD
11, 4167–4198, 2011

For the presented paper, we combine data sets for the time period 2001 to 2010 as derived from measurements at different emission lines. For water vapour, the measurements of the 489 GHz emission line provide 119 690 profiles covering altitudes between 20 km and 75 km (here we use only stratospheric data up to 50 km), and the measurements of the 557 GHz emission line provide 132 572 profiles covering altitudes between 50 km and 100 km. The two data sets are matched by setting the values at 50 km to the mean of the values at 49 km and 51 km and by applying a 3-point running mean between 48 km and 52 km. For stratospheric ozone, measurements of the 544 GHz emission line provide 600 667 profiles covering altitudes between 20 km and 75 km. As for mesospheric water vapour information, the temperature field was derived from the measurements of the 557 GHz band which provide therefore also 132 572 temperature profiles covering altitudes between 50 km and 90 km. Overall, the data profile densities represent a horizontal resolution of about 1200 irregularly spaced data profiles per month for water vapour and temperature and about 5600 irregularly spaced data profiles per month for ozone for the time period of June 2001 to April 2010. The vertical resolution provided by the retrievals is ~3–3.5 km for water vapour, ~2–3 km for ozone and ~4–5 km for temperature (Urban et al., 2005; Lossow et al., 2007). For data handling all of the profiles are interpolated to a grid with vertical resolution of 1 km.

Firstly we construct seasonal means by sampling the irregularly spaced Odin data profiles on a $10^\circ \times 10^\circ$ latitude-longitude grid. Then the zonally asymmetric components O_3^*, H_2O^* and T^* are derived. The Odin temperature profiles are combined with ERA-Interim temperature profiles (1000 hPa–1 hPa) for the same time period using the same sampling procedure on a $10^\circ \times 10^\circ$ grid. We match the two data sets at stratopause altitudes (~50 km) analogously to the procedure of the two water vapour data profiles mentioned above, but by setting the values around 50 km to the mean values of 48 km and 52 km excluding very strong differences between temperatures at the lowermost level of Odin temperature data at 50 km and at the upper level of the ERA-Interim at 1 hPa.

ACPD
11, 4167–4198, 2011

2.2 Zonal asymmetries in ozone and water vapour

Figure 1.1–1.2 and Figure 2.1–2.2 show zonally asymmetric ozone (O_3^*) and water vapour (H_2O^*) for different seasons at 60° N and at 60° S. Note here that the maxima and minima of stratospheric wave one structures can be found mostly at the edge of the winter polar vortex, i.e. at latitudes around 60° N or 60° S. During northern winter the amplitudes of the wave one patterns are about 10–20% of zonal mean values.

Figure 1.1 illustrates that, in the Northern Hemisphere, the wave one pattern builds up during autumn (SON: September, October, November), maintains during winter (DJF: December, January, February) and decays during spring (MAM: March, April, May). During summer (JJA: June, July, August) there are only minor planetary wave patterns in the lower stratosphere which might be due to zonal asymmetries in eddy mixing processes in the upper troposphere/lower stratosphere (UTLS) region induced by synoptic-scale baroclinic waves. Both the double-peak structure in O_3^* occurring during winter and the fact that the wave one pattern of O_3^* do not show a westward shift in phase with increasing height, as usually found in other quantities like temperature and geopotential height, are not well understood up to now. We assume that, to first order, O_3^* is controlled mainly dynamically by transport processes in the lower stratosphere where its chemical lifetime is long, but controlled mainly chemically in the upper stratosphere where its chemical lifetime is short. In the UTLS region, we assume a contribution of zonal asymmetries in eddy mixing processes because they are particularly strong during winter and because their effect on temperature and ozone distribution is quite strong at these altitudes (e.g., Bartels et al., 1998; Gabriel and Schmitz, 2003). In the upper stratosphere, the temperature-dependent NO_x($NO_x = NO + NO_2$) catalytic ozone destruction cycle becomes more important for ozone changes because of higher mean temperatures (Stolarski and Douglass, 1985; Flury et al., 2009), therefore zonal asymmetries in the NO_x cycle may be important in contributing to the wave pattern in ozone at these altitudes. Consistently O_3^* is then correlated with temperature in the lower stratosphere but anti-correlated in the upper stratosphere.

ACPD
11, 4167–4198, 2011

In the Southern Hemisphere a wave one structure in O_3^* develops mainly during southern spring (SON) when the polar vortex breaks up, as shown in Fig. 1.2. Here we have to consider that the southern winter polar vortex is usually much more stable and more zonally symmetric than the northern winter polar vortex, and that the final break-up during spring occurs usually later in Southern than in Northern Hemisphere. As for Northern Hemisphere, zonal asymmetries in O_3^* during southern summer (DJF) may be related to zonal asymmetries in eddy mixing processes induced by synoptic-scale baroclinic waves.

In the Northern Hemisphere, H_2O^* shows also a pronounced wave one pattern during autumn and winter, but up to mesosphere and with a strong jump in phase at upper stratosphere altitudes (Fig. 2.1). In the Southern Hemisphere, the wave one pattern develops mainly during southern spring when the polar vortex breaks up (Fig. 2.2, SON), similarly to O_3^*. In order to understand the jump in phase at upper stratosphere one has to consider that the mean concentrations of H_2O increase from about 2 ppm at lower stratosphere to about 5–6 ppm at upper stratosphere/lower mesosphere altitudes, but then decrease with increasing height in the mesosphere (e.g., Randel et al., 1998; Urban et al., 2007), and that therefore the mean horizontal and vertical gradients of H_2O change in sign at upper stratosphere/lower mesosphere altitudes. Thus we assume that the spatial structure of H_2O^* may be mainly generated by zonal asymmetries in meridional transport or Brewer-Dobson circulation, with the phase shift being related to the change in sign of the mean horizontal ($[H_2O]_y$) and vertical ($[H_2O]_z$) gradients (where $[H_2O]$ is zonal mean and the subscripts y and z denote the derivations in latitude and height) at upper stratosphere/lower mesosphere altitudes. This assumption will be confirmed below when analysing the transport equation.

In the upper troposphere/lower stratosphere (UTLS) region, the stationary wave patterns in H_2O may also be generated by zonal asymmetries in temperature-dependent oxidation of CH_4, in water vapour depletion by $O(^1D)$, and in eddy mixing processes due to tropospheric baroclinic wave activity. Quasi-stationary planetary wave patterns in the stratosphere induce zonal asymmetries in gravity wave propagation, which then

ACPD
11, 4167–4198, 2011

contribute to quasi-stationary waves patterns in mesospheric geopotential, as suggested by Smith (2003). Associated zonal asymmetries in residual circulation and eddy mixing processes induced by gravity wave breaking may therefore also contribute to the wave pattern in mesospheric water vapour. Wave one patterns in H_2O are found also for northern summer (JJA) and southern summer (DJF) but mainly at mesosphere altitudes, which may also be due to zonal asymmetries in gravity wave breaking, e.g. in connection with gravity wave generation due to orography or due to storm tracks over the ocean basins.

2.3 Zonal asymmetries in T^* and geostrophically balanced dynamics

Figure 3.1 shows the zonally asymmetric temperature T^* at 60° N during winter, together with the zonally asymmetric geopotential height Φ^* derived via:

$$\frac{\partial \phi}{\partial z} = -\frac{RT}{H} \tag{1}$$

(with $\Phi = \phi/g$, ϕ: geopotential, g: gravity acceleration of the earth, $H = 7500$ m and $\phi = 0$ for the standard pressure level 1000 hPa as lower boundary). Figure 3.1 shows also the meridional geostrophic wind v_g derived via:

$$v_g = \frac{1}{f}\frac{\partial \phi}{\partial x} \tag{2}$$

(with f: Coriolis parameter; note that $[v_g] = 0$), and, as follows from steady-state quasi-geostrophically balanced equation for potential temperature $d_g\theta + w\theta_{0z} = Q$ (with $d_g = \partial_t + \underline{\boldsymbol{v}}_{\boldsymbol{g}}\nabla$, $\partial_t\theta = 0$, $\underline{\boldsymbol{v}}_{\boldsymbol{g}} = (u_g, v_g)$, $u_g = -\Phi_y/f$, $\theta_0 = \theta_0(z)$ and $Q^* = 0$), the zonally asymmetric geostrophically-balanced vertical wind component w_b^* derived via:

$$w_b^* = -([u_g]\frac{\partial \theta^*}{\partial x} + v_g^*\frac{\partial [\theta]}{\partial y} + D^*)/\frac{\partial \theta_0}{\partial z} \tag{3}$$

where $D^* = (u_g^*\theta^*)_x + (v_g^*\theta^*)_y - [v_g^*\theta^*]_y$ denotes the zonally asymmetric component of eddy fluxes (note that $[u_g^*\theta^*]_x = 0$; subscripts t, x, y and z denote the derivations with

ACPD
11, 4167–4198, 2011

time, longitude, latitude and height). Here we neglect the zonally asymmetric component in radiative forcing Q^* when deriving w_b^*, although it may have an additional influence on the amplitude and phase of the wave one pattern in the order of 10–20%, as suggested by several model studies (e.g., Gabriel et al., 2007; Gillet et al., 2009). However, for a first-order approximation of mean transport characteristics this approach seems to be acceptable.

At 60° N, the westward shift in phase of T^* (Fig. 3.1a) corresponds to a westward shift in geopotential height anomaly Φ^* (Fig. 3.1b), i.e. there is a polar low anomaly over North Atlantic/Europe and a high anomaly over the Aleutians. Consequently there are zonally asymmetric wave one patterns in the geostrophically balanced meridional and vertical winds (Fig. 3.1c, d), with poleward winds at the eastern flank of the polar low anomaly and equatorward winds at the western flank of the polar low anomaly, indicating strong zonal asymmetries in meridional tracer transport.

A similar wave one pattern is found in the Southern Hemisphere at 60° S during autumn, but with weaker amplitude (Fig. 3.2). A westward shift in phase of T^* (Fig. 3.2a) corresponds to a westward shift in geopotential height anomaly Φ^* (Fig. 3.2b), with a southern polar low anomaly centred at around 30° W and a high anomaly centred at around 150° E at altitudes of ~40 km. As in northern winter, there are subsequently poleward winds at the eastern flank of the southern polar low anomaly and equatorward winds at the western flank of the southern polar low anomaly (note here the reversed sign of Coriolis force), which also indicate strong zonal asymmetries in meridional tracer transport. The remarkable similarity in phase of northern and southern wave one pattern might be due to similarities in planetary-scale orography (e.g., the north-southward direction of Rocky Mountains/Andes mountain ridge extending over both Northern and Southern Hemisphere) or due to similarities in the differences in tropospheric wave activity over the Pacific and over the Atlantic/Indian ocean basins.

In the following we analyse the effect of v_g^* and w_b^* on the stationary wave patterns in O_3^* and H_2O^* based on a simplified tracer transport equation. Note here that we derived also other non-geostrophic wind components via Phillips approximation ($u_{ag} = (d_g v_g)/f$

ACPD
11, 4167–4198, 2011

and $v_{ag} = (d_g u_g)/f$ with steady state conditions $\partial_t = 0$ and $|f| > 0$ for the extra-tropics) and residual winds via $f v_{res} = [v_g^* q_g^*]$ from quasi-geostrophic potential vorticity fluxes (with $q_g = f - u_{gy} + v_{gx} + f(\theta^*/\theta_{0z})_z$ and $(v_{res})_y + (w_{res})_z = 0$). However, the effect of these ageostrophic components on the stationary wave patterns in O_3^* and H_2O^* turns out to be at least one order of magnitude smaller than those of v_g^* and w_b^* and are not considered here. A shortcoming is, of course, that the ageostrophic and residual winds were only derived from the stationary flow pattern, because the derivation of transient flow patterns is not possible due the restrictions in the temporal and spatial resolution of the Odin data. Furthermore, the impact of gravity waves on the residual circulation is not included. Nevertheless, we expect a first order result when analyzing the effect of the stationary quasi-geostrophically-balanced flow.

3 Simplified meridional transport for zonally asymmetric tracer components

Based on the transport equation for a tracer $\mu = [\mu] + \mu^*$:

$$\frac{d\mu}{dt} = \frac{\partial \mu}{\partial t} + \underline{\boldsymbol{v}} \nabla \mu = S \tag{4}$$

(where $\boldsymbol{v} = (u, v, w)$ and S: chemical sources), the derived winds are used to estimate the transport tendencies for the zonally asymmetric component $\mu^* = \mu - [\mu]$

$$\frac{\partial \mu^*}{\partial t} + \underline{\boldsymbol{v}} \nabla(\mu^*) = S^* + G^* - D^* \tag{5}$$

with $G^* = -v^* \partial\, [\mu]_y - w^* \partial [\mu]_z$ and zonally asymmetric components of eddy fluxes $D^* = D - [D] = (u^* \mu *)_x + (v^* \mu^*)_y + (w^* \mu^*)_z - [v^* \mu^*]_y - [w^* \mu^*]_z$ and chemical sources $S^* = S - [S]$. Here, the generation term G^* gives a contribution to the tendency of μ^* as a function of zonal mean tracer distribution $[\mu]$ and zonal asymmetries in meridional and vertical winds v^* and w^*. Applying our approximation of the winds from Sect. 2.3, we find that $G_g^* = -v_g^* [\mu]_y - w_b^* [\mu]_z$ (for illustration, Fig. 4.1 and 4.2 shows G_g^* for O_3^* and H_2O^* at 60° N) is stronger than the eddy flux terms by approximately one order.

ACPD
11, 4167–4198, 2011

When comparing Fig. 4.1 with Fig. 3.1, and considering that $[O_3]_y < 0$ and $[O_3]_z < 0$ in middle and upper stratosphere, it is evident that we find positive tendencies $G_g^*(O_3^*)$ at these levels in regions of poleward winds at the eastern flank of polar low anomaly and negative tendencies in regions of southward winds at the western flank of polar low anomaly. We can also understand the positive and negative tendencies $G_g^*(H_2O^*)$ if we consider the change in sign of both the meridional and vertical gradients of zonal mean water vapour at stratopause altitudes (i.e. $[H_2O]_y > 0$ and $[H_2O]_z > 0$ for h<50 km and $[H_2O]_y < 0$ and $[H_2O]_z < 0$ for $h > 50$ km), which is therefore responsible for the strong jump in phase of the wave one structure at these altitudes in case of zonally asymmetric wind components v_g^* and w_b^*.

As far as we derived advection by ageostrophic winds from quasi-geostrophically balanced equations as described in Sect. 2.3, we find that these terms are of second importance in comparison to the advection by zonal mean westerlies, i.e. $u_{ag}\mu_x^* << [u_g]\mu_x^*$, $v_{ag}\mu_y^* << [u_g]\mu_x^*$ and $w^*\mu_z^* << [u_g]\mu_x^*$. Of course, the non-balanced ageostrophic components and the eddy fluxes may be underestimated because they are derived based on only long-term mean stationary and quasi-geostrophically balanced wave components, neglecting interannual variations of the stationary components and transient waves. In the middle stratosphere, stationary waves may be usually larger than transient waves, but in the lower stratosphere zonal asymmetries in transient wave activity contribute largely to the eddy transport processes (Gabriel and Schmitz, 2003; Haklander et al., 2008). Also above the stratopause transient waves may become more important. However, in the framework of the presented paper the non-balanced ageostrophic components and the transient wave activity cannot be quantified because of the limitations of the temporal and spatial Odin data profile density.

Now we assume that, to a first order, the term $G_g^*(\mu^*)$ is balanced by the advection of μ^* within the zonal mean westerlies $[u_g]$, i.e. based on a first order approximation of the transport equation (assuming steady state: $\partial\mu_t/\mu = 0$ and neglecting zonally asymmetric source term for an inert tracer: $S^* = 0$) we can formulate:

ACPD
11, 4167–4198, 2011

$$\frac{d\mu^*}{dt} \approx [u_g]\frac{\partial \mu^*}{\partial x} \approx G_g^* = -v_g^*\frac{\partial [\mu]}{\partial y} - w^*\frac{\partial [\mu]}{\partial z} \quad (6)$$

A specific solution of Eq. (6) $\mu^* = \mu^*(\mathrm{TR})$ can be derived via Fourier transformation:

$$\mu_x^* \approx G_g^*/[u_g] \Rightarrow \mu^* = \Sigma c_k e^{ikx}, \text{with } \mu_x^* = \Sigma ikc_k e^{ikx} \text{and } G_g^*/[u_g] = \Sigma C_k e^{ikx} \quad (7)$$

and comparison of coefficients ($ikc_k = C_k$) for horizontal wave numbers k and regions where $[u_g] > 0$ (which is usually fulfilled in the extra-tropics from upper troposphere to mesosphere except during summer months; in order to avoid unrealistic values in $G_g^*/[u_g]$ we use $1/[u_g] \approx [u_g]/([u_g]^2 + \varepsilon)$ with $\varepsilon = 1\,\mathrm{ms}^{-1}$).

The resulting fields $O_3^*(\mathrm{TR})$ and $H_2O^*(\mathrm{TR})$ at 60° N for northern autumn and winter are plotted in Fig. 5.1 and 5.2, which show – as a first-order approach – similar wave one patterns like those of observed O_3^* and H_2O^* shown in Figs. 1.1 and 2.1. In particular, the simple transport approach captures the correct phase of the zonal asymmetries, but it underestimates their amplitudes nearly by a factor of 2 and do not capture specifics like the double-peak structure in stratospheric O_3^*. These differences may be due to zonally asymmetric components in chemical loss and production rates and/or in additional transport processes due to transient waves, which cannot be derived based on Odin data alone. However, we conclude that a large fraction of the zonal asymmetries in O_3^* and H_2O^* can be explained by zonal asymmetries in mean meridional transport by geostrophically balanced winds, which are related to position, strength and spatial structure of northern polar low and Aleutian high anomalies.

In the Southern Hemisphere, the fields $O_3^*(\mathrm{TR})$ and $H_2O^*(\mathrm{TR})$ at 60° S (Fig. 5.3 and 5.4) show also a wave one pattern similar to those observed (compare with Figs. 1.2 and 2.2), but only during southern spring (SON), with weaker amplitudes and less outspread, i.e. the regions of pronounced values are spatially more concentrated to middle stratosphere ($O_3^*(\mathrm{TR})$) or middle stratosphere and lower mesosphere ($H_2O^*(\mathrm{TR})$). As for Northern Hemisphere, the differences between the observed fields and the fields derived by the simplified transport approach illustrate additional effects contributing to

ACPD
11, 4167–4198, 2011

the stationary wave patterns, e.g., zonal asymmetries in temperature-dependent chemistry and eddy mixing processes due to transient waves.

When comparing the winter means of observed (Figs. 1.1 and 2.1) and derived (Fig. 5.1 and 5.2) mixing ratios, the processes which contribute to the stationary wave patterns can be addressed more specifically. For example, the combined influence of zonal asymmetries in baroclinic wave activity and associated eddy mixing processes in the UTLS region and of zonal asymmetries in temperature-dependent NO_x chemistry in the upper stratosphere may be responsible for the double peak structure in O_3^*, modifying the mean wave one pattern as described by the simplified approach of Eq. (6). Zonal asymmetries in eddy mixing of tropospheric CH_4 into stratosphere, in temperature-dependent CH_4-oxidation, which is the main source of H_2O in the stratosphere, and in water vapour depletion by $O(^1D)$ may contribute to the amplitude of the stationary wave patterns in stratospheric H_2O. In the upper stratosphere and mesosphere, the planetary wave one pattern affects gravity wave propagation and gravity wave breaking, which may contribute to zonal asymmetries in both eddy mixing and residual circulation and, hence, to the mean amplitude of the stationary wave pattern in mesospheric H_2O^*. This would be consistent with model-based investigations of stationary wave patterns in mesospheric geopotential height and temperature (e.g., Smith, 2003). In the southern lower stratosphere (Figures 1.2 and 2.2), the effect of heterogeneous chemistry on the surface of Polar Stratospheric Cloud (PSC) droplets lead to strong ozone depletion within the polar vortex during southern spring when temperatures are very low (e.g. WMO, 2007), therefore zonal asymmetries in the southern polar vortex will contribute to the wave one pattern in O_3^* via zonal asymmetries in PSC occurrence and related heterogeneous chemistry. A similar contribution to the stationary wave one in ozone may be expected concerning zonal asymmetries in the northern polar vortex, although it may be weaker because temperatures inside the northern polar vortex are usually not as low as inside the southern polar vortex.

ACPD
11, 4167–4198, 2011

4 Summary and discussion

Based on long-term means of ozone and water vapour profiles derived from Odin satellite data 2001–2010, we find a pronounced wave one pattern in the zonally asymmetric components of both stratospheric ozone $O_3^* = O_3$-[O_3] and stratospheric and mesospheric water vapour $H_2O^* = H_2O$-[H_2O] in the Northern and in the Southern Hemisphere ([O_3], [H_2O]: zonal means). In the Northern Hemisphere, the wave one patterns increase during autumn, maintain their strength during winter and decay during spring, with maximum amplitudes of about 10–20% of zonal mean values. In the Southern Hemisphere, the wave one pattern develops mainly during southern spring when the southern stratospheric polar vortex breaks up. Based on a simplified approach of transport equation for an inert tracer, we showed that the stationary wave patterns are largely related to zonal asymmetries in the time mean of meridional transport by geostrophically balanced winds, in relation to position, strength and spatial structure of low and high anomalies in geopotential height, e.g., in relation to northern winter polar low and Aleutian high anomalies. In particular, our transport approach captures the correct phase of the quasi-stationary wave patterns in O_3^* and H_2O^* but underestimates their amplitudes nearly by a factor of 2. Also the observed double-peak structure in stratospheric O_3^* during northern winter with peak amplitudes in lower and in upper stratosphere is not reproduced by the transport approach. Therefore we have to consider additional transport processes or chemical sources contributing to the stationary wave patterns in O_3^* and H_2O^* which are not included in the simplified approach.

Transient wave activity or eddy mixing processes due to baroclinic waves or gravity waves may be important in configuring the stationary wave patterns, but they cannot be quantified in the framework of the presented paper because of the temporal and spatial limitations of the Odin satellite profile density. Also zonal asymmetries in temperature-related chemistry cannot be derived from the Odin data alone. However, when comparing the stationary wave patterns in ozone and water vapour observed by Odin and derived by the simplified transport approach, the possible influence of

ACPD
11, 4167–4198, 2011

these processes can be addressed more specifically. On the one hand, zonal asymmetries in baroclinic wave activity and associated eddy mixing processes in the UTLS region may contribute to the mean amplitude of lower stratospheric O_3^*, whereas zonal asymmetries in temperature-dependent NO_x chemistry may contribute to the mean amplitude of upper stratospheric O_3^*, with the combination resulting in the double peak structure of O_3^*. On the other hand, zonal asymmetries in eddy mixing of tropospheric CH_4 into lower stratosphere and/or in temperature-dependent CH_4-oxidation and water vapour depletion by $O(^1D)$ may contribute to the mean amplitude of stratospheric H_2O^*, whereas zonal asymmetries in gravity wave breaking and associated zonal asymmetries in eddy mixing and residual circulation may contribute to the mean amplitude in mesospheric H_2O^*.

The stationary planetary wave patterns derived from the satellite data are a suitable indicator of the processes generating these patterns, i.e. zonal asymmetries in meridional transport processes. It is important to understand and to quantify these processes because they play a key role in understanding longitudinal differences in wave-driven transports and in the atmospheric circulation, and because they provide an important validation tool for predictions with general circulation models (GCMs) and chemistry-climate models (CCMs) in the framework of ozone depletion and climate change scenarios. Quantifying the stationary wave patterns in ozone and water vapour may also be important because of the feedbacks to wave propagation and atmospheric circulation via the induced radiation perturbations, as suggested by a number of recent model studies (Gabriel et al., 2007; Crook et al., 2008; Gillet et al., 2009; Waugh et al., 2009). Our results therefore suggest further investigations of the processes generating the stationary wave patterns based on both observations and CCMs.

ACPD
11, 4167–4198, 2011

Acknowledgements. Odin is a Swedish-led satellite project funded jointly by the Swedish National Space Board (SNSB), the Canadian Space Agency (CSA), the National Technology Agency of Finland (Tekes) and the Centre National d'Etudes Spatiales (CNES) in France. The Swedish Space Corporation has been the industrial prime constructor. Since April 2007 Odin is a third-party mission of ESA. The work of the presented paper was supported by the German Research Foundation (DFG – Deutsche Forschungsgemeinschaft).

References

Andrews, D. G., Holton, J. R., and Leovy, C. B.: Middle Atmosphere Dynamics, International Geophysical Series, vol. 40, Academic Press, 489 pp., 1987.

Austin, J. and Butchart, N.: A 3-dimensional modeling study of the influence of planetary wave dynamics on polar ozone photochemistry, J. Geophys. Res., 97, 10165–10186, 1992.

Bartels, J., Peters, D., and Schmitz, G.: Climatological Ertel's potential-vorticity flux and mean meridional circulation in the extratropical troposphere – lower stratosphere, Ann. Geophys., 16, 250–265, 1998, http://www.ann-geophys.net/16/250/1998/.

Brasseur, G. and Solomon, S.: Aeronomy of the Middle Atmosphere, D. Reidel Publishing Company, Dordrecht (Netherlands), 445 p., 1995.

Charney, J. and Drazin, P.: Propagation of planetary-scale disturbances from the lower into the upper atmosphere, J. Geophys. Res., 66, 83–109, 1961.

Crook, J. A., Gillett, N. P., and Keeley, S. P. E.: Sensitivity of Southern Hemisphere climate to zonal asymmetry in ozone, Geophys. Res. Lett., 35, L07806, doi:10.1029/2007GL032698, 2008.

Flury, T., Hocke, K., Haefele, A., Kämpfer N., and Lehmann, R.: Ozone depletion, water vapor increase, and PSC generation at midlatitudes by the 2008 major stratospheric warming, J. Geophys. Res., 114, D18302, doi:10.1029/2009JD011940, 2009.

Gabriel, A. and Schmitz, G.: The Influence of Large-Scale Eddy Flux Variability on the Zonal Mean Ozone Distribution, J. Climate, 16, 2615–2627, 2003.

Gabriel, A., Peters, D., Kirchner, I., and Graf, H.-F.: Effect of zonally asymmetric ozone on stratospheric temperature and planetary wave propagation, Geophys. Res. Lett., 34, L06807, doi:10.1029/2006GL028998, 2007.

ACPD

11, 4167–4198, 2011

Gillett, N. P., Scinocca, J. F., Plummer, D. A., and Reader, M. C.: Sensitivity of climate to dynamically consistent zonal asymmetries in ozone, Geophys. Res. Lett., 36, L10809, doi:10.1029/2009GL037246, 2009.

Haklander, A. J., Siegmund, P. C., Sigmond, M., and Kelder, H. M.: How does the northern-winter wave driving of the Brewer-Dobson circulation increase in an enhanced-CO2 climate simulation?, Geophys. Res. Lett., 35, L07702, doi:10.1029/2007GL033054. 2008.

Holton, J. R.: Meridional distribution of stratospheric trace gas constituents, J. Atmos. Sci., 43, 1238–1243, 1986.

Holton, J. R. and Gettelman, A.: Horizontal transport and the dehydration of the stratosphere, Geophys. Res. Lett., 28, 2799-2802, 2001.

Hood, L. and Zaff, D.: Lower stratospheric stationary waves and the longitude dependence of ozone trends in winter, J. Geophys. Res., 100, 25791–25800, 1995.

Jones, A., Urban, J., Murtagh, D. P., Eriksson, P., Brohede, S., Haley, C., Degenstein, D., Bourassa, A., von Savigny, C., Sonkaew, T., Rozanov, A., Bovensmann, H., and Burrows, J.: Evolution of stratospheric ozone and water vapour time series studied with satellite measurements, Atmos. Chem. Phys., 9, 6055–6075, doi:10.5194/acp-9-6055-2009, 2009.

Joshi, M. M., Charlton, A. J., and Scaife, A. A.: On the influence of stratospheric water vapour changes on the tropospheric circulation, Geophys. Res. Lett., 33, L09806, doi:10.1029/2006GL025983, 2006.

Kinnersley, J. S. and Tung, K.-K.: Modeling the Global Interannual Variability of Ozone Due to the Equatorial QBO and to Extratropical Planetary Wave Variability, J. Atmos. Sci., 55, 1417–1428, 1998.

Karpetchko, A., Kyro, E., and Knudsen, B. M.: Arctic and Antarctic polar vortices 1957–2002 as seen from the ERA-40 reanalyses, J. Geophys. Res., 110, D21109, doi:10.1029/2005JD006113, 2005.

Lossow, S., Urban, J., Eriksson, P., Murtagh, D., and Gumbel, J.: Critical parameters for the retrieval of mesospheric water vapour and temperature from Odin/SMR limb measurements at 557 GHz, Adv. Space Res., 40, 835–845, 2007.

Lossow, S., Urban, J., Gumbel, J., Eriksson, P., and Murtagh, D.: Observations of the mesospheric semi-annual oscillation (MSAO) in water vapour by Odin/SMR, Atmos. Chem. Phys., 8, 6527–6540, doi:10.5194/acp-8-6527-2008, 2008.

Lossow, S., Urban, J., Schmidt, H., Marsh, D. R., Gumbel, J., Eriksson, P., and Murtagh, D.: Wintertime water vapor in the polar upper mesosphere and lower thermosphere: First

ACPD
11, 4167–4198, 2011

satellite observations by Odin submillimeter radiometer, J. Geophys. Res.,114, D10304, doi:10.1029/2008JD011462, 2009.

Murtagh, D., Frisk, U., Merino, F., Ridal, M., Jonsson, A., Stegman, J., Witt, G., Eriksson, P., Jimenez, C., Mégie, G., de La Noëë, J., Ricaud, P., Baron, P., Pardo, J.-R., Hauchecorne, A., Llewellyn, E. J., Degenstein, D. A., Gattinger, R. L., Lloyd, N. D., Evans, W. F. J., McDade, I. C., Haley, C., Sioris, C., von Savigny, C., Solheim, B. H., McConnell, J. C., Strong, K., Richardson, E. H., Leppelmeier G. W., , Kyrölä, E., Auvinen H., and Oikarinen, L.: An overview of the Odin Atmospheric Mission, Can. J. Phys., 80, 309–319, 2002.

Peters, D. and Entzian, G.: January ozone anomaly over the North Atlantic-European region: Longitude-dependent decadal change in the total ozone during 1979–1992, Meteorol. Zeitschrift, 5, 41–44, 1996.

Peters, D. and Entzian, G.: Longitude-dependent decadal changes of total ozone in boreal winter months during 1979–1992, J. Climate, 12, 1038–1048, 1999.

Peters, D. H. W., Gabriel, A., and Entzian, G.: Longitude-dependent decadal ozone changes and ozone trends in boreal winter months during 1960-2000, Ann. Geophys., 26, 1275–1286, doi:10.5194/angeo-26-1275-2008, 2008.

Randel, W. J., Wu, F., Russell III, J. M., Roche, A., and Waters, J. W.: Seasonal cycles and QBO variations in stratospheric CH_4 and H_2O observed in UARS HALOE data, J. Atmos. Sci., 55, 163–185, 1998.

Sassi, F., Boville, B. A., Kinnison, D., and Garcia, R. R.: The effects of interactive ozone chemistry on simulations of the middle atmosphere, Geophys. Res. Lett., 32, L07811, doi:10.1029/2004GL022131, 2005.

Smith, A. K.: The Origin of Stationary Planetary Waves in the Upper Mesosphere, J. Atmos. Sci., 60, 3033–3041, 2003.

Solomon, S., Portmann, R. W., Garcia, R. R., Randel, W., Wu, F., Nagatani, R., Gleason, J., Thomason, L., Poole, L. R., and McCormick, M. P.: Ozone depletion at midlatitudes: Coupling of volcanic aerosols and temperature variability to anthropogenic chlorine, Geophys. Res. Lett., 25, 1871–1874, 1998.

SPARC Assessment of Upper Tropospheric and Stratospheric Water Vapour, edited by: Kley, D., Russell III, J. M., and Phillips, C., SPARC Report No. 2, WCRP – 113, WMO/TD – No. 1043, http://www.atmosp.physics.utoronto.ca/SPARC, 2002.

Stolarski, R. S., and Douglass, A. R.: Parameterization of the photochemistry of stratospheric ozone including catalytic loss processes, J. Geophys. Res., 90, 10709–10718, 1985.

ACPD
11, 4167–4198, 2011

Tung, K.-K.: On the Two-Dimensional Transport of Stratospheric Trace Gases in Isentropic Coordinates, J. Atmos. Sci., 39, 2330–2355, 1982.

Urban, J., Lautié, N., Le Flochmoën, E., Jiménez, C., Eriksson, P., de La Noëë, J., Dupuy, E., Ekström, M., El Amraoui, L., Frisk, L. U., Murtagh, D., Olberg M., and Ricaud, P.: Odin/SMR limb observations of stratospheric trace gases: Level 2 processing of ClO, N_2O, HNO_3, and O_3, J. Geophys. Res., 110, D14307, doi:10.1029/2004JD005741, 2005.

Urban, J., Lautié, N., Murtagh, D. P., Eriksson, P., Kasai, Y., Lossow, S., Dupuy, E., de La Noë, J., Frisk, U., Olberg, M., Le Flochmoën, E., and Ricaud, P.: Global observations of middle atmospheric water vapour by the Odin satellite: An overview, Planet. Space Sci., 55(9), 1093–1102, 2007.

Waugh, D. W., and Randel, W. J.: Climatology of Arctic and Antarctic polar vortices using elliptical diagnostics, J. Atmos. Sci., 56, 1594–1613, 1999.

Waugh, D. W., Oman, L., Newman, P. A., Stolarski, R. S., Pawson, S., Nielsen, J. E., and Perlwitz, J.: , Effect of zonal asymmetries in stratospheric ozone on simulated Southern Hemisphere climate trends, Geophys. Res. Lett., 36, L18701, doi:10.1029/2009GL040419, 2009.

WMO (World Meteorological Organization): Scientific Assessment of Ozone Depletion: 2006, Global Ozone Research and Monitoring Project – Report No. 50, 572 pp., Geneva, 2007.

ACPD
11, 4167–4198, 2011

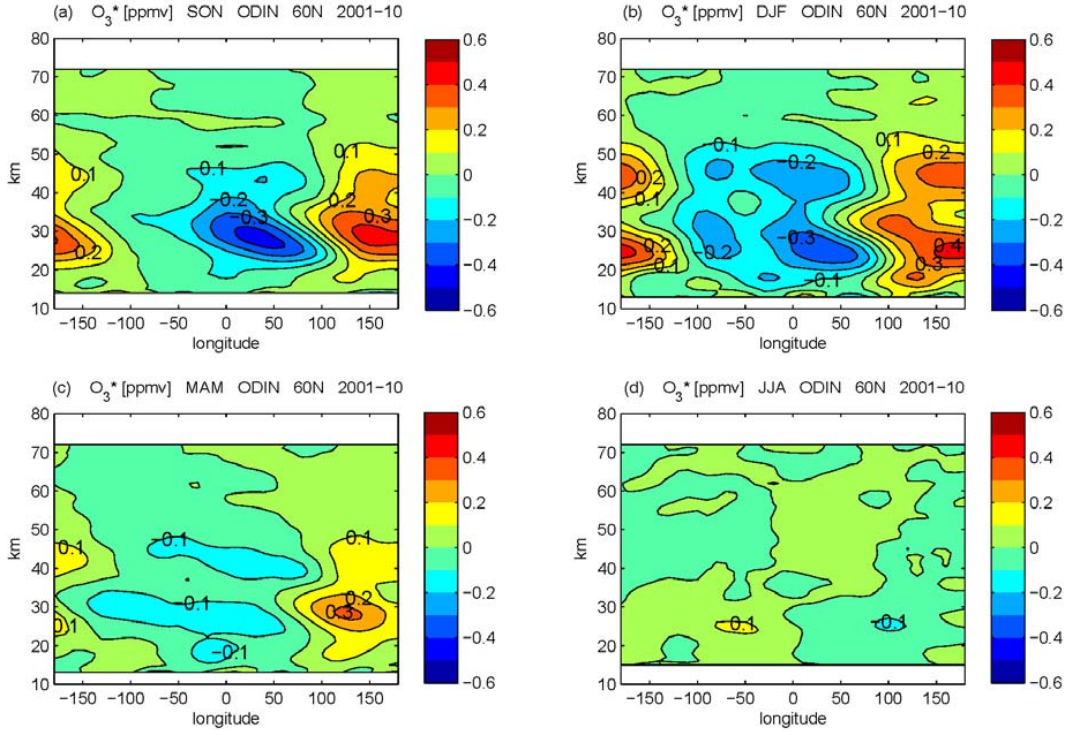

Fig. 1.1. Long-term means of the zonally asymmetric component in volume mixing ratio of ozone $O_3^* = O_3\text{-}[O_3]$ (in ppm: parts per million) at 60° N for different seasons of the time period 2001–2010; **(a)** autumn (SON: September-October-November), **(b)** winter (DJF: December-January-February), **(c)** spring (MAM: March-April-May) and **(d)** summer (JJA: June-July-August); distance of isolines: 0.1 ppmv.

ACPD
11, 4167–4198, 2011

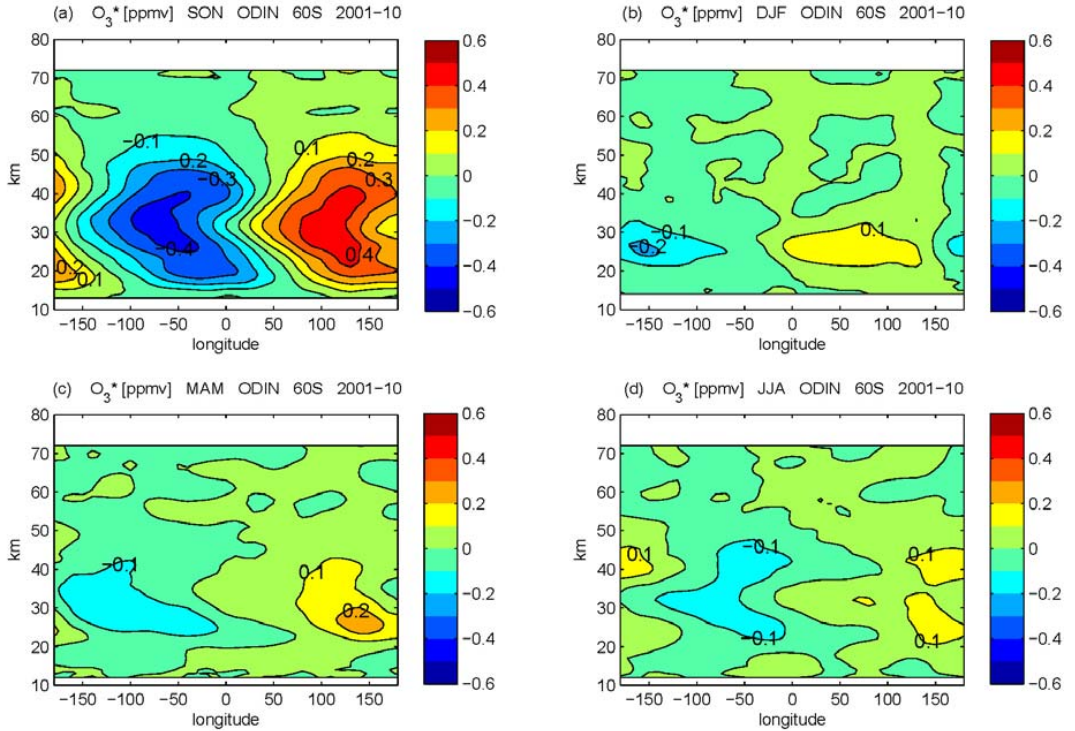

Fig. 1.2. Long-term means of zonally asymmetric ozone O_3^* for different seasons as in Fig. 1.1, but at 60° S.

ACPD
11, 4167–4198, 2011

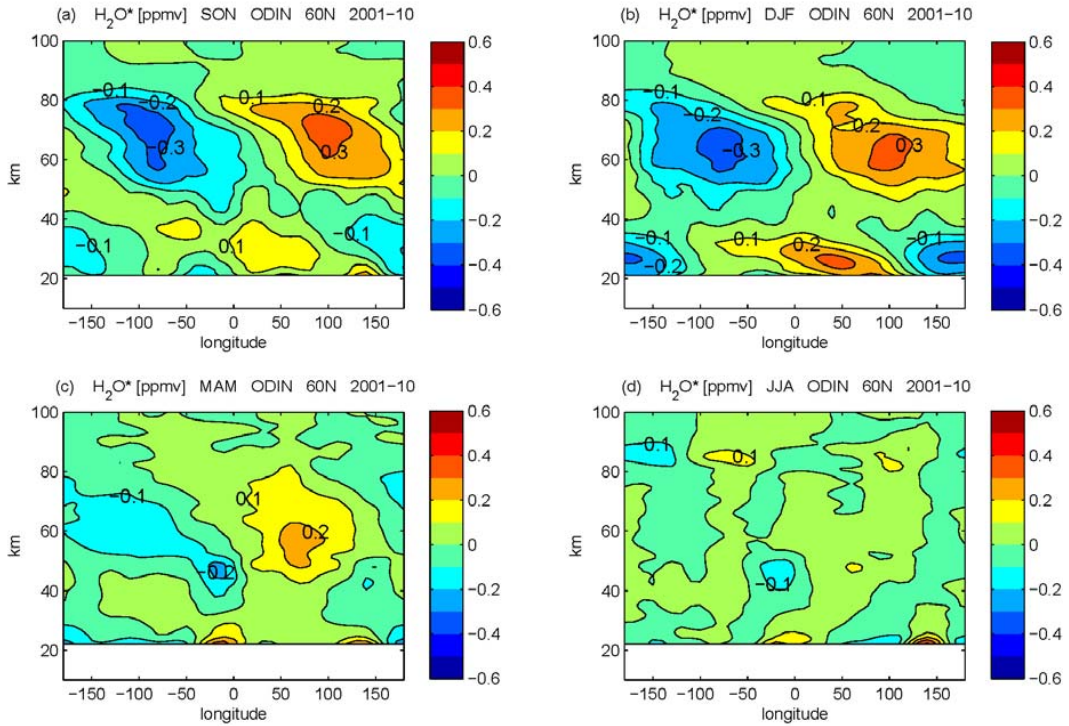

Fig. 2.1. Long-term means of the zonally asymmetric component in volume mixing ratio of water vapour $H_2O^* = H_2O\text{-}[H_2O]$ (in ppm: parts per million) at 60° N for different seasons of the time period 2001–2010; **(a)** autumn (SON: September-October-November), **(b)** winter (DJF: December-January-February), **(c)** spring (MAM: March-April-May) and **(d)** summer (JJA: June-July-August); distance of isolines: 0.1 ppmv.

ACPD
11, 4167–4198, 2011

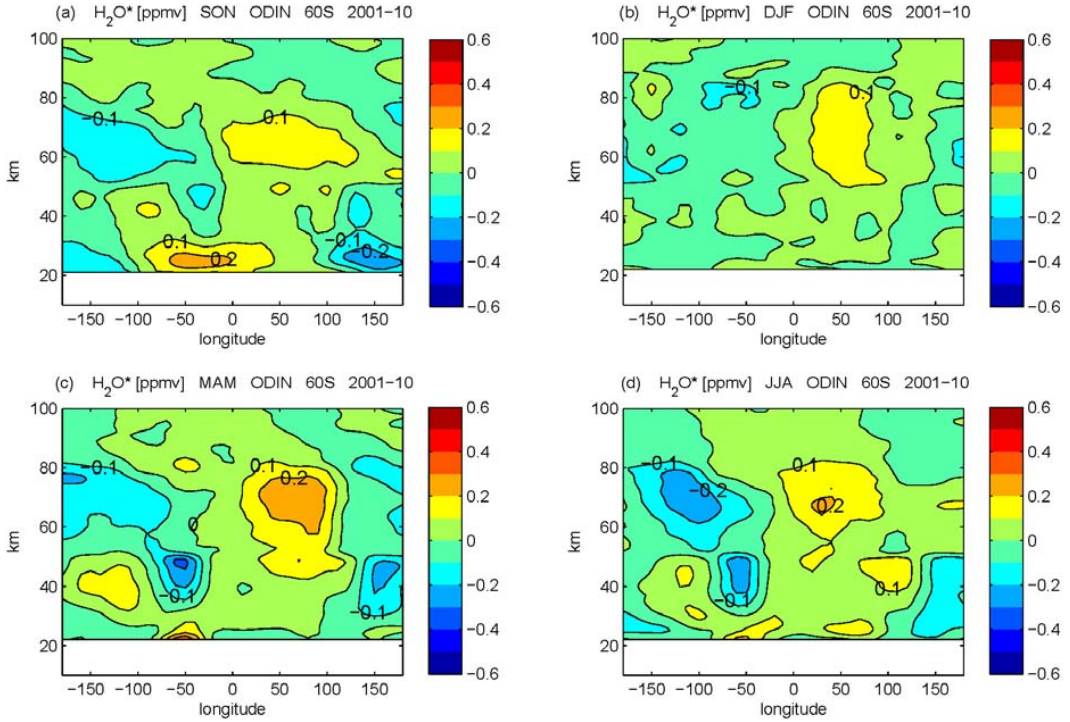

Fig. 2.2. Long-term means of zonally asymmetric water vapour H_2O^* for different seasons as in Fig. 2.1, but at 60° S.

ACPD
11, 4167–4198, 2011

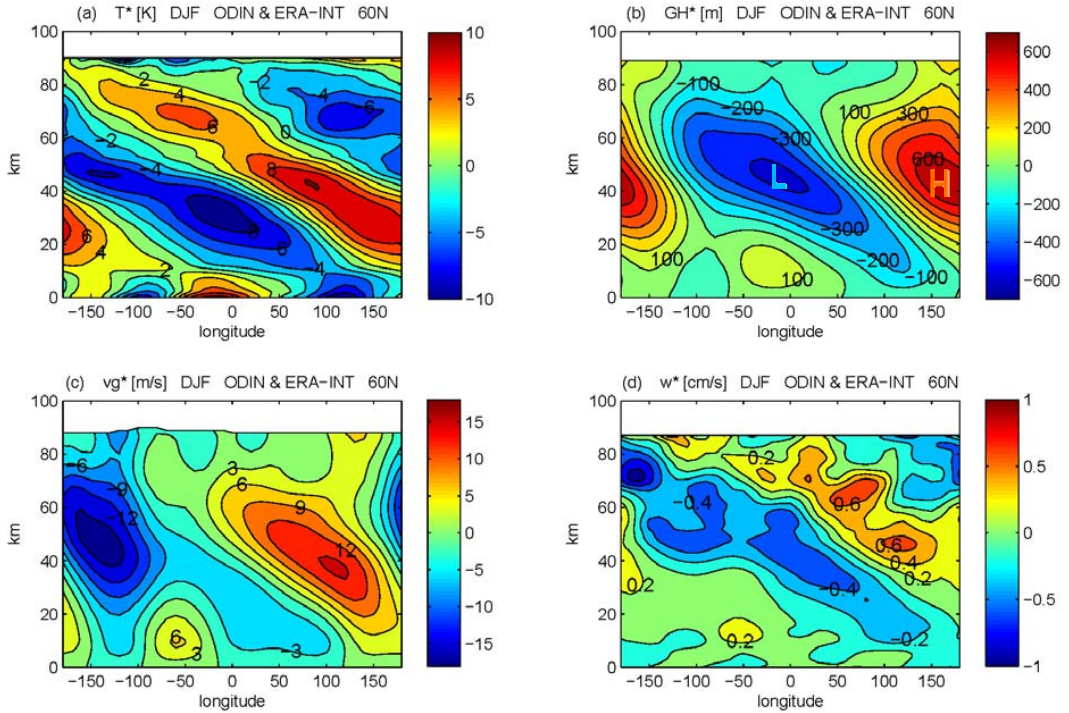

Fig. 3.1. Long-term means of zonally asymmetric components of **(a)** temperature T^* (isolines in K), **(b)** geopotential height Φ^* (GH^*, isolines in m), **(c)** meridional geostrophic wind v_g^* (isolines in ms^{-1}) and **(d)** geostrophically-balanced vertical wind w^* (isolines in cms^{-1}) at 60° N for northern winter (DJF) of the time period 2001–2010, derived from combined Odin satellite data (50–100 km) and ERA Interim data (0–50 km).

ACPD
11, 4167–4198, 2011

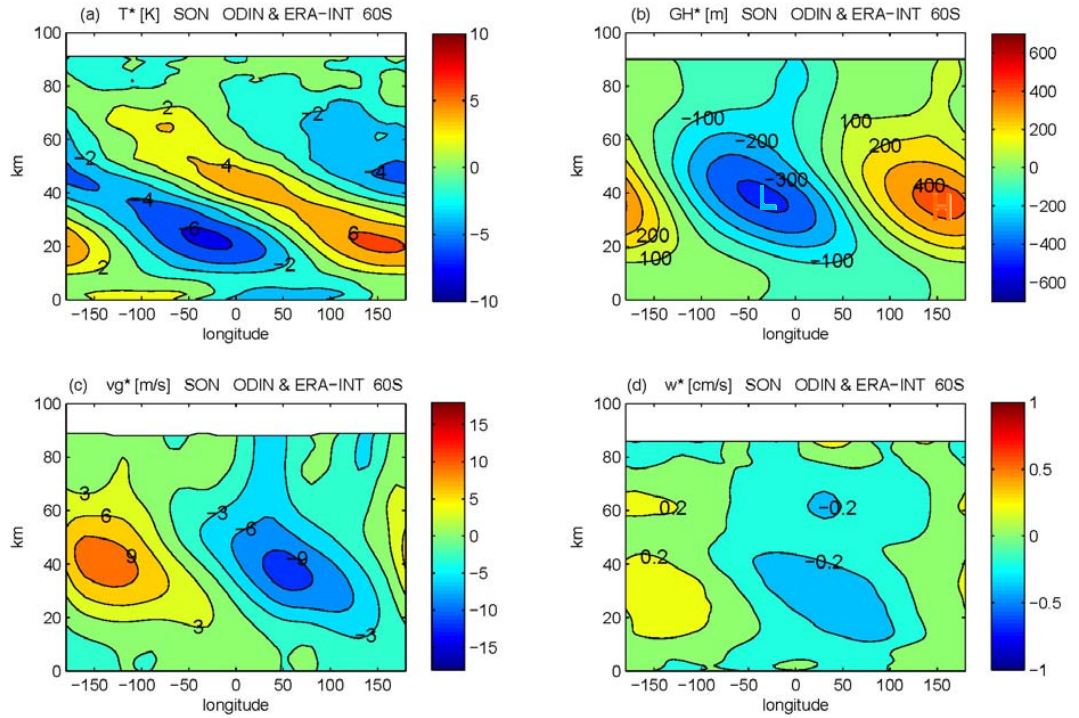

Fig. 3.2. Long-term means of T^*, Φ^*, v_g^* and w^* as in Fig. 2.1, but at 60° S.

ACPD
11, 4167–4198, 2011

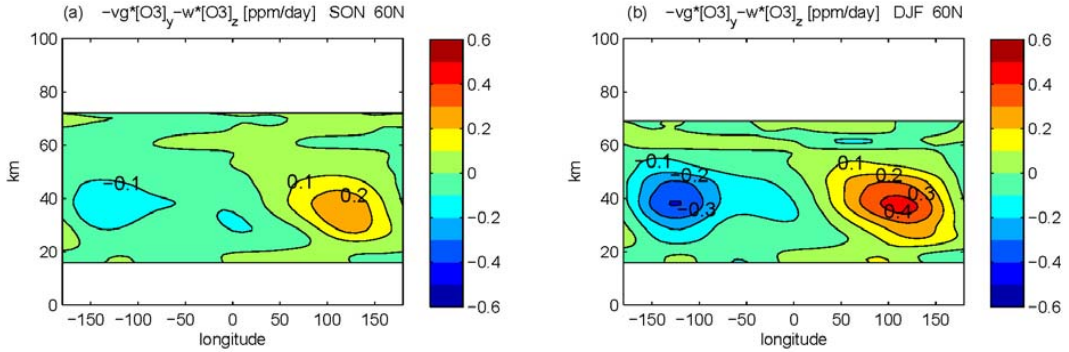

Fig. 4.1. Mean transport tendency term $G_g^*(O_3^*) = -v_g^*[O_3]_y - w^*[O_3]_z$ (in ppm per day) for **(a)** autumn and **(b)** winter at 60° N, as derived from mean ozone and mean geostrophically-balanced winds of the time period 2001–2010 (details see Sect. 3); distance of isolines: 0.1 ppmv day^{-1}.

ACPD
11, 4167–4198, 2011

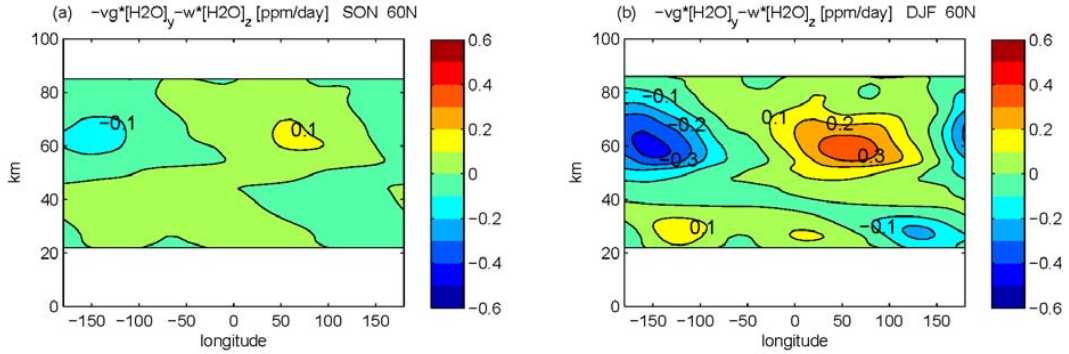

Fig. 4.2. Mean transport tendency term $G_g^*(H_2O^*) = -v_g^*[H_2O]_y - w^*[H_2O]_z$ (in ppm per day) for **(a)** autumn and **(b)** winter at 60° N, as derived from mean water vapour and mean geostrophically-balanced winds of the time period 2001–2010 (details see Sect. 3); distance of isolines: 0.1 ppmv day^{-1}.

ACPD
11, 4167–4198, 2011

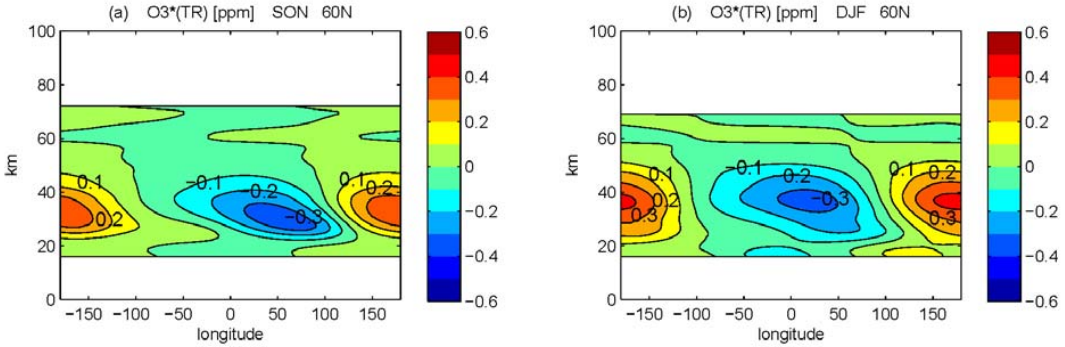

Fig. 5.1. First order solutions $O_3^*(TR)$ (in ppm) derived via simplified transport relation $(O_3^*(TR))_x \approx G_g^*(O_3^*)/[u_g]$ (details see Sect. 3) for **(a)** autumn and **(b)** winter of the time period 2001–2010 at 60° N; distance of isolines: 0.1 ppmv.

ACPD
11, 4167–4198, 2011

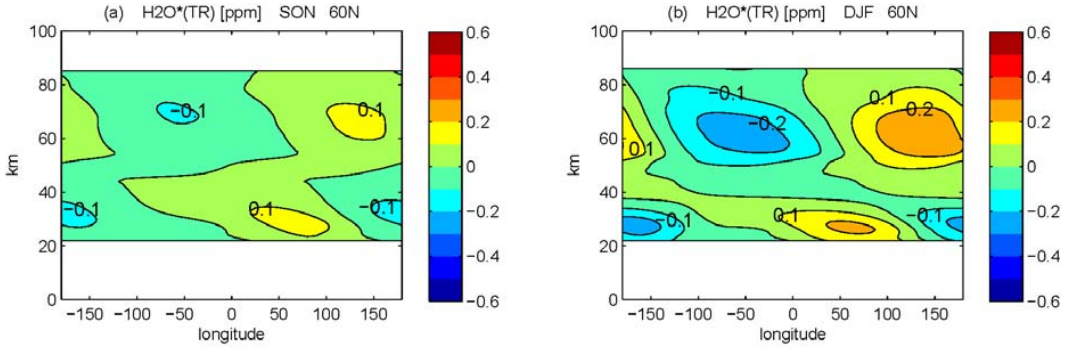

Fig. 5.2. First order solutions $H_2O^*(TR)$ (in ppm) derived via simplified transport relation $(H_2O^*(TR))_x \approx G_g^*(H_2O^*)/[u_g]$ (details see Sect. 3) for **(a)** autumn and **(b)** winter of the time period 2001–2010 at 60° N; distance of isolines: 0.1 ppmv.

ACPD
11, 4167–4198, 2011

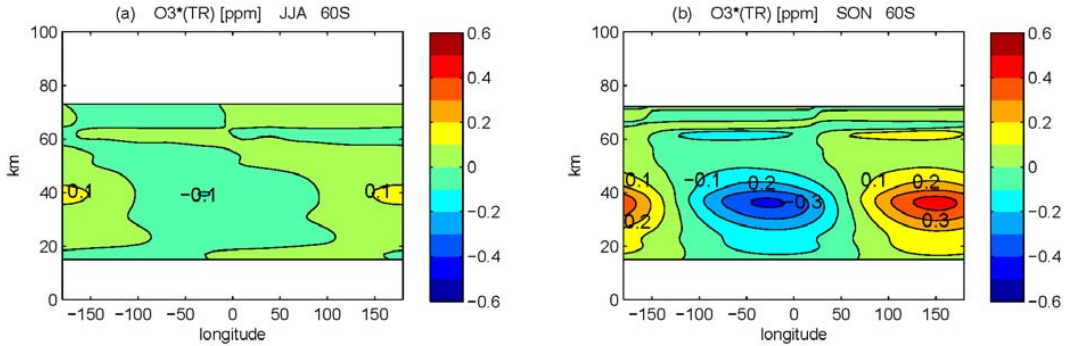

Fig. 5.3. First order solutions $O_3^*(TR)$ as in Fig. 5.1, but for 60° S.

ACPD
11, 4167–4198, 2011

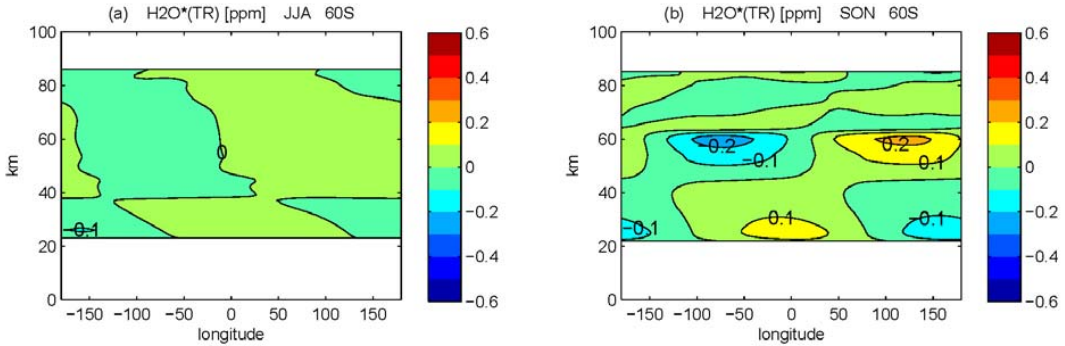

Fig. 5.4. First order solutions H_2O^*(TR) as in Fig. 5.2, but at 60° S.

ACPD
11, 4167–4198, 2011